Solar Phys (2008) 248: 395–408
DOI 10.1007/s11207-007-9005-7

The Pixelised Wavelet Filtering Method to Study Waves and Oscillations in Time Sequences of Solar Atmospheric Images

R.A. Sych · V.M. Nakariakov

Received: 30 April 2007 / Accepted: 11 July 2007 / Published online: 21 August 2007

Abstract Pixelised wavelet filtering (PWF) for the determination of the spatial, temporal, and phase structure of oscillation sources in temporal sequences of 2D images, based upon the continuous wavelet transform, has been designed and tested. The PWF method allows us to obtain information about the presence of propagating and nonpropagating waves in the data and localise them precisely in time and in space. The method is tested on the data sets obtained in microwaves with the Nobeyama Radioheliograph and in the EUV with TRACE. The method reveals fine spatial structuring of the sources of 3-, 5-, and 15-minute periodicities in the microwave and EUV emission generated in sunspot atmospheres. In addition, the PWF method provides us with unique information about the temporal variability of the power, amplitude, and phase narrowband maps of the observed oscillations and waves. The applicability of the method to the analysis of coronal wave phenomena is discussed.

1. Introduction

Wave and oscillatory phenomena are believed to play a crucial role in a number of physical processes operating in the atmosphere of the Sun and Sun-like stars (*e.g.,* Nakariakov and Verwichte, 2005). However, the analysis of solar data to determine parameters of atmospheric waves and oscillations is a nontrivial task, mainly because these phenomena lie near the very threshold instrumental detectability, necessitating the analysis of spatial, temporal, and phase variability at the highest possible resolution. The commissioning of the modern generation of high spatial- and temporal-resolution solar observational instruments (*e.g.,* the Nobeyama Radioheliograph (NoRH), the *Transition Region and Coronal Explorer* (TRACE), and instruments onboard the *Solar and Heliospheric Observatory* (SOHO)) stimulated the development of novel data analysis methods, such as multiscale wavelet analysis

R.A. Sych (✉)
Institute of Solar-Terrestrial Physics, 126 Lermontov St., Irkutsk, Russia
e-mail: sych@iszf.irk.ru

V.M. Nakariakov
Physics Department, University of Warwick, Coventry CV4 7AL, UK
e-mail: V.Nakariakov@warwick.ac.uk

(MWA) (Meyer and Roques, 1993), the empirical mode decomposition method (EMD), the complex empirical orthogonal function (CEOF) method (Huang, Shen, and Long, 1999), singular spectrum analysis (SSA) (Golyandina, Nekrutkin, and Zhiglyavsky, 2001), and multifractal analysis (Milovanov and Zelenyj, 1993). The interest of these methods is motivated by the transient and localised nature of the solar atmospheric oscillations.

One of the intrinsic properties of solar coronal and low-atmospheric wave and oscillatory phenomena is the pronounced temporal modulation of the wave parameters, *e.g.* of the amplitude and period, and also their transient nature. A popular tool allowing researchers to study wave phenomena of this kind is the wavelet-transform technique. This method has been intensively used in solar atmospheric physics for the past decade. In particular, Baudin, Bocchialini, and Koutchmy (1996) applied wavelets to the study of oscillations in the chromospheric network; Ireland *et al.* (1999) studied intensity oscillations in active regions observed with SOHO/CDS. Recently, wavelet analysis was applied to the analysis of longitudinal waves observed over sunspots with TRACE and other instruments (De Moortel, Hood, and Ireland, 2002; King *et al.*, 2003; Marsh *et al.*, 2003). Also, Christopoulou *et al.* (2003) considered temporal evolution of the velocity and intensity oscillations in sunspot umbrae at the chromospheric level.

The study presented here proposes and tests a novel method of pixelised wavelet filtering (PWF) for the study of spatially-distributed oscillation sources in the solar atmosphere. In this work, we follow Torrence and Compo (1998) and use the continuous wavelet transform with the Morlet mother function. The PWF method is based upon the application of the wavelet transform to the construction of narrowband and broadband static and dynamical spectral 2D maps of the analysed temporal sequences of 2D images (data cubes). One of the main aims of this work is the development and testing of an analytical tool for the determination of the fine spatial structure of transient oscillation sources and interrelations of the spectral peaks revealed by the analysis of the spatially-integrated signal. To the temporal signal of each pixel of the spatial field of view, we apply wavelet filtration to decompose the signal in the temporal domain (temporal frequencies) and determine the spatial distribution of the power of different spectral components in a way to allow study of the temporal evolution of the spatial–frequency information. This analysis allows us to obtain narrowband maps (associated with a certain chosen periodicity), to determine the wave type (propagating or nonpropagating in the field of view), and to study their temporal evolution.

The developed method is similar to two other previously-used approaches to the analysis of wave phenomena in solar atmospheric imaging data sets, the wavelet-based oscillation detection technique developed by De Moortel and McAteer (2004) and the EMD- and CEOF-based methods applied by Terradas, Oliver, and Ballester (2004). The PWF method discussed in this paper differs from these methods in the following aspects:

i) In PWF, one can prescribe precisely the frequency boundaries of the analysed spectral band. It is possible to analyse either a chosen discrete harmonic or a prescribed band of continuous frequencies.
ii) A possible outcome of PWF is a 2D map showing the spatial distribution of the amplitude, power, and phase of selected narrowband signals (*narrowband maps*).
iii) It is possible to study the temporal evolution of the narrowband maps, by considering the variation of the amplitude, power, and phase of selected narrowband signals (*dynamical narrowband maps*). In particular, this allows one to estimate the projected phase speed of the waves.
iv) The method, in contrast with the EMD and COEF methods, provides us with the flexibility in the choice of the mother wavelet function as well as in the frequency – time resolution of the wavelet filtering.

v) The PWF technique can be readily developed to the calculation of the cross-correlation spectra, allowing for the study of the interaction of wave and oscillatory processes contained in different data cubes. In particular, these data cubes can be obtained with different instruments and/or in different wavelengths.

Some of these features can be obtained with the methods of De Moortel and McAteer (2004) and Terradas, Oliver, and Ballester (2004), but not simultaneously with the same analytical tool. The unique feature of the PWF method is the construction of the dynamical narrowband maps (item *iii*). In particular, the method of De Moortel and McAteer, designed for the automated detection of temporal periodicities and of their spatial distribution, allows us to identify the presence of a periodicity in the signal associated with a given spatial spectrum, but it does not give us its temporal evolution. For example, the PWF method allows us to determine the number of periods in the detected oscillation and the evolution of the signal in the spectral band of interest.

We apply the PWF method to the analysis of sunspot and coronal loop oscillations, using the well-known data cubes obtained with NoRH (17 GHz, already discussed by Gelfreikh *et al.*, 1999) and with TRACE (171 Å, discussed by De Moortel, Ireland, and Walsh, 2000, and by Terradas, Oliver, and Ballester, 2004). The aim was to reproduce the previous findings and to demonstrate the applicability of the PWF method to the analysis of coronal imaging data cubes.

2. Test Signals

The input signal is a data cube that consists of a sequence of 2D images sampled with a specified temporal cadence. In particular, it can be an EUV data cube obtained with SOHO/EIT or TRACE EUV imagers, *Hinode*/XRT or *Yohkoh*/SXT imagers, or with NoRH. The data cubes obtained with different instruments have their own intrinsic features; thus it is worth testing the general applicability of the PWF method with an artificial synthetic data cube.

In the test, analogous to the test signal applied by Terradas, Oliver, and Ballester (2004) for the CEOF method, the simulated data cube consists of 300 21 × 21 pixel frames. The temporal cadence is one second. The synthetic data cube contains a superposition of a standing and upwards and downwards propagating monochromatic waves of different periods, wavelengths, and amplitudes:

$$X_{\sum}(x, y, t) = X_{\mathrm{SW}}(x, y, t) + X_{\mathrm{UTW}}(x, y, t) + X_{\mathrm{DTW}} + N(x, y, t), \tag{1}$$

where x and y are the spatial coordinates, t is time,

$$X_{\mathrm{SW}}(x, y, t) = 2 \sin\left(\frac{2\pi x}{15}\right) \times \sin\left(\frac{2\pi t}{100}\right) \times \exp\left[\frac{y-10}{4}\right]^2, \tag{2}$$

$$X_{\mathrm{UTW}}(x, y, t) = 4 \sin 2\pi\left(\frac{x}{12} - \frac{t}{60}\right) \times \exp\left[\frac{y-17}{2}\right]^2, \tag{3}$$

$$X_{\mathrm{DTW}} = 4 \sin 2\pi\left(\frac{x}{4} + \frac{t}{20}\right) \times \exp\left[\frac{y-3}{2}\right]^2, \tag{4}$$

and $N(x, y, t)$ is a high-frequency noise. The standing wave has a period of 100 arbitrary units, an amplitude of 2, and a wavelength of 15. In the following we assume that the temporal units in the test signal are seconds; hence the period is 100 seconds. The propagating

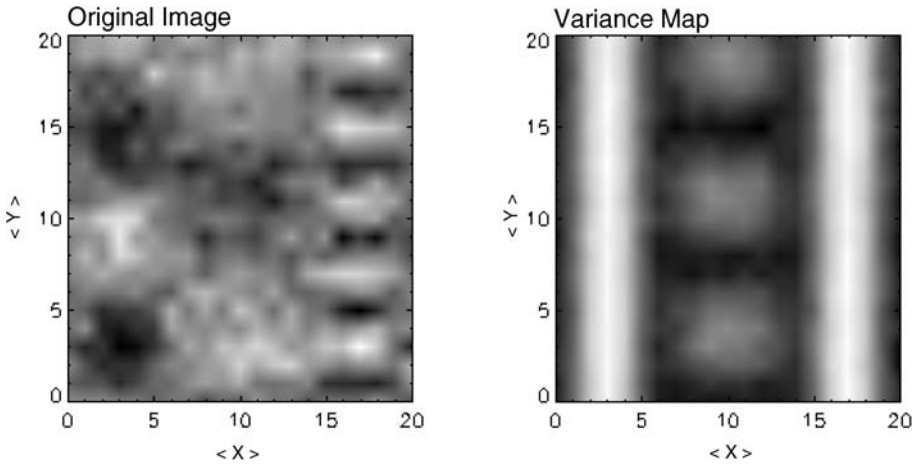

Figure 1 Left: A 2D snapshot of the test signal, which contains a standing and two propagating monochromatic waves and noise. Right: The variance map showing the spatial distribution of the oscillation power for the whole time sample. It is possible to see two vertical strips of Gaussian shape, corresponding to the propagating waves, and three maxima, corresponding to the standing wave.

waves have amplitude 4, periods of 60 and 20 seconds, and wavelengths of 12 and 4 units, respectively, and are localised at different parts of the image. A snapshot of the signal is shown in the left panel of Figure 1.

3. The Scheme of the Pixelised Wavelet Filtering Method

The PWF method is based upon the wavelet transform described by detail in Weng and Lau (1994) and Torrence and Compo (1998). In this work, as the mother wavelet function, we use the complex Morlet wavelet, which is well localised in both the spectral domain characterised by the spectral coordinate ω (the frequency) and the physical domain characterised by the coordinate t (the time):

$$\Psi(t) = \exp(\mathrm{i}\omega t)\exp\left(-t^2/2\right), \tag{5}$$

which is a monochromatic wave modulated by a Gaussian of unit width.

As a first step, we identify the region of interest (ROI) for the subsequent analysis. In particular, we may obtain information about the spatial distribution of the temporal variations including all spectral frequencies by constructing a broadband variance map based upon the temporal variance of each pixel. For this purpose, we calculate mean-square variations from the mean value for each pixel and make a contour-plot map of the analysed field of view (FOV). The map shows the spatial distribution of the power of all spectral components in the FOV (a similar technique was developed by Grechnev, 2003). The variance maps allow us to select the ROI for further analysis. The variance map of test signal (1) is shown in the right panel of Figure 1. We point out that the variance map does not contain any information about the localisation of the event of interest in time.

As the next step, we determine the significant frequencies of the studied oscillations and the time intervals showing the oscillations with these frequencies. We calculate the wavelet spectrum of the temporal signal integrated over the whole ROI. Figure 2 shows the integrated

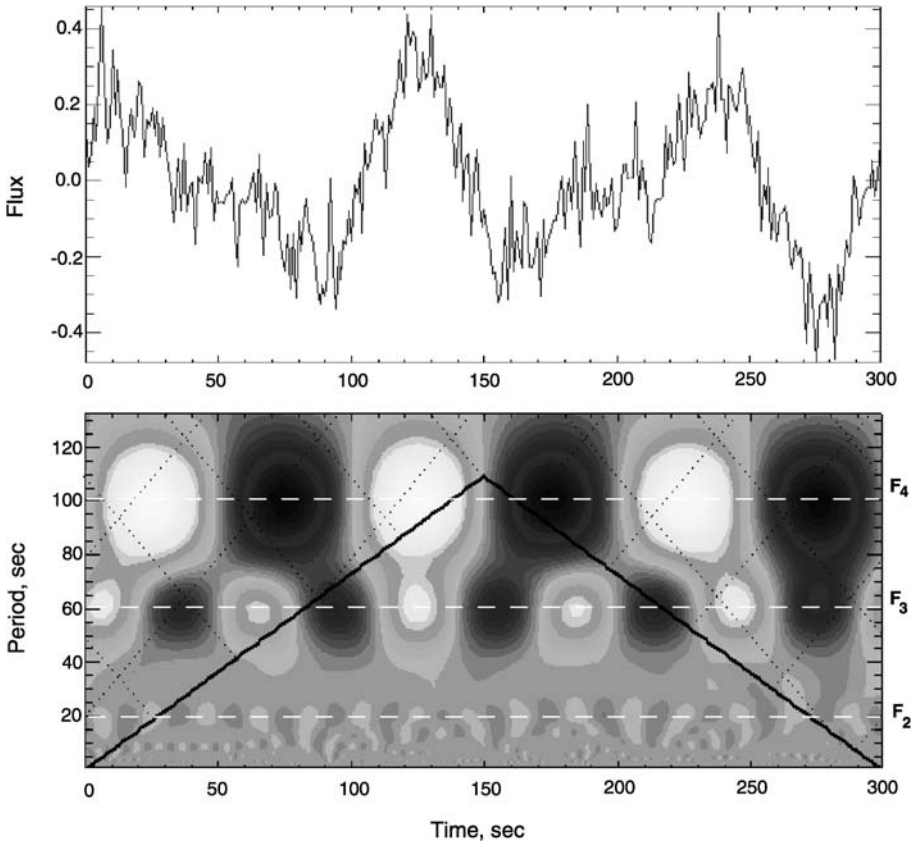

Figure 2 Upper panel: Time signal integrated over the field of view. Bottom panel: Amplitude wavelet of the signal given in the upper panel. The horizontal dashed lines show the built-in periods.

wavelet spectrum of the synthetic data cube described in Section 2. The built-in periodicities are well seen in the spectrum.

Similar wavelet spectra are constructed for all individual pixels, obtaining a 4D data cube given by two spatial axes, the time axis and the frequency axis. Then, for each frequency of interest (built-in, identified in the integrated wavelet spectrum, or just assumed to be in the signal), for each pixel, we make the inverse wavelet transform. Thus, we obtain temporal variations of the narrowband signals in the vicinity of the frequency of interest at every pixel, with all other frequencies filtered out. Repeating this for each frequency of interest (or for all frequencies), we obtain a set of temporal variations for each pixel. The number of curves is determined by the number of frequencies in the discrete spectrum, which in turn is determined by the number of frames in the analysed data cube.

Then, we determine the power of each of the obtained narrowband curves as an integral over time of the mean-square deviation (variance) from its mean. Repeating this procedure for each pixel we obtain the spatial distribution of the power associated with this particular frequency. The obtained data cube formed by the frequency and two spatial axes (*broadband power cube*) can be used for the visualisation of the spatial distribution of the spectrum of the oscillation sources. The left panel of Figure 3 shows the broadband power cube of the analysed synthetic data set, highlighting the built-in wave motions in the analysed test signal.

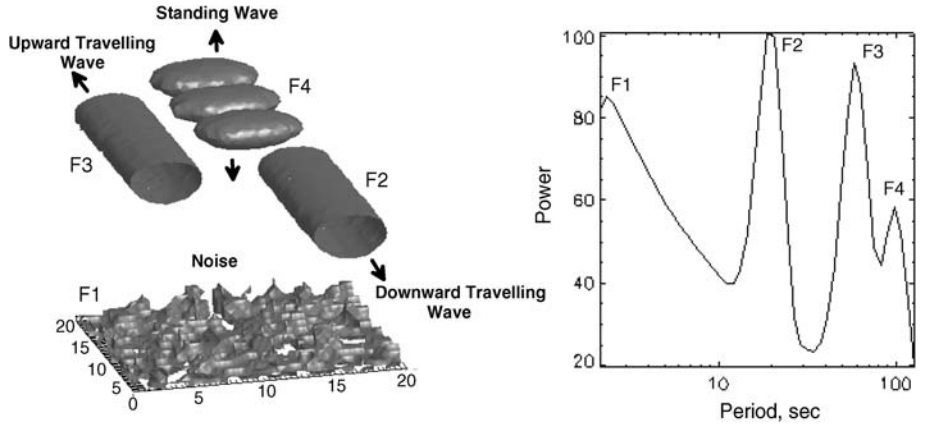

Figure 3 Left: The spatial distribution of the signal power of different built-in waves (the broadband power cube). The vertical axis (not shown) corresponds to the periods and shows the detected periodicity: 20-, 60-, and 100-second monochromatic signals and the noise. Right: Spatially integrated global wavelet power spectrum of the analysed time sequences of 2D images.

The morphological features of the waves are clearly seen in Figure 3: the standing waves have well-defined periodically spaced shapes corresponding to their extremes, whereas the propagating waves are cylinders of elliptical cross section, resulting from averaging the wave profiles. The high-frequency noise is uniformly distributed over the space.

Taking the spatial distribution of the power associated with a certain frequency (or integrated over a certain frequency band) we obtain a *narrowband power map* for the frequency or band of interest. In Figure 3 (left panel), this corresponds to slicing the 3D frequency – spatial cube in the horizontal direction, perpendicular to the vertical axis representing the frequency.

Using this spatial distribution and integrating the narrowband temporal signals over the spatial domain for each frequency we obtain the *global spatially integrated wavelet power spectrum* (an analogue of the Fourier power spectrum) of the analysed data cube, which is shown in the right panel of Figure 3. There are three distinct peaks in the spectrum, corresponding to the built-in 20-, 60-, and 100-second periodicities, as well as high-frequency noise.

Similarly, using the phase spectrum instead of the amplitude one, we get information about the phase of the signal. The phase is obtained by calculating separately the real and imaginary parts of the signal.

One of the disadvantages of the broadband and narrowband power maps is the lack of temporal information, as the signal is integrated over time. Using the values of the significant periods found in the global wavelet spectrum (Figure 3, right panel) we can study the temporal evolution of the spatial sources of these oscillations, making movies of the narrowband maps calculated at different instants of time (*dynamical narrowband maps*). The duration of the analysed temporal interval is determined by the width of the mother wavelet function. A snapshot of the dynamical map gives us the spatial distribution of the amplitude or phase of the signal in the frequency band of interest (or at a prescribed harmonic) at a particular instant of time (a *narrowband map*). Sequences of narrowband maps give us the temporal evolution of the periodicity of interest.

Figure 4 shows amplitude and phase narrowband maps of the analysed data cube at three different instants of time. The crosses on the image show the positions of the extrema in the

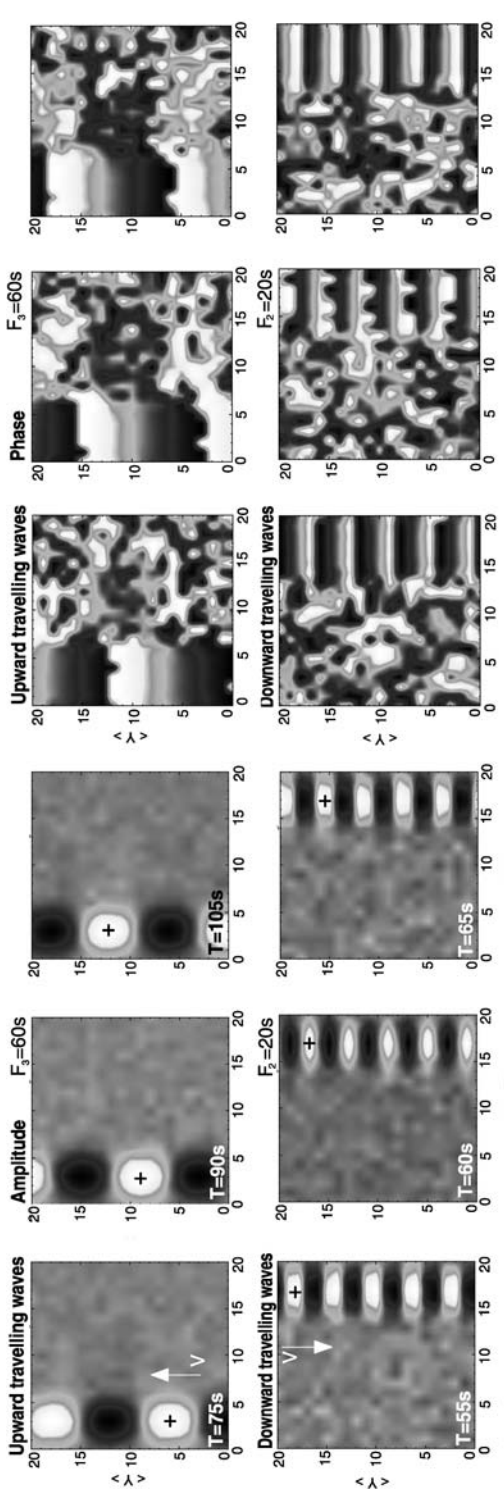

Figure 4 Sequences of amplitude narrowband maps of the synthetic data cube, showing the temporal variation of the amplitude and phase of the narrowband oscillation sources of upward and downward propagating waves with periods of 60 and 20 second (upper and middle panels, respectively) and of standing waves with a period of 100 second (bottom panel). The corresponding spatial distribution of the wave phases (the phase narrowband maps) are shown in the right panels. The crosses show the wave extrema. The arrows show the direction of the wave propagation.

signal. It is seen that the positions of the extrema of the standing waves (Figure 4, bottom panel) do not change in time, whereas their amplitudes do. Also, the phase of standing waves is seen to change in a period (Figure 4, right panel). The extrema of the propagating waves (with periods of 20 and 60 seconds) are seen to move in time (Figure 4, upper and middle panels). A movie constructed with the use of all frames shows the upwards and downwards propagating waves, clearly in agreement with the test signal.

Thus, the test demonstrates the applicability of the PWF method to the identification of the nature of harmonic or quasi-harmonic oscillations and waves in imaging data cubes. In particular, the method allows one to distinguish confidently between standing and propagating waves. We point out that in the analysis of natural data cubes, the projection effect should be taken into account. The phase speed of the "propagating" waves is the speed projected on the FOV plane. The term "standing" is applied to the waves that do not propagate in the FOV plane. However, the wave can be propagating in the direction of the line of sight.

4. Application to Sunspot Oscillations

We process the microwave observations of sunspots, obtained with NoRH at 17 GHz on 22 July 1994, 30 June 1993, and 16 August 1992, with a temporal cadence of 10 seconds and a spatial resolution $10''$ in the circular-polarisation channel $V = R - L$. In those data sets, the shortest detectable period is 30 seconds, and the longest detectable period is about 1000 s. The data have already been analysed by Gelfreikh *et al.* (1999) and were found to contain oscillations of the integrated radio flux with periods of 120 – 220 and 300 seconds. Here, we apply the PWF method for determining the spatial distribution and evolution of the dominating spectral harmonics in this data set.

The data sets were preprocessed with the use of the Solar Soft (SSW) IDL routines norh_trans and norh_synth. The images were co-aligned with each other to get rid of high-frequency jitter and their calibration. For this purpose, we use align_cube_correl.

The broadband variance maps of the events, aimed at localising the regions with maximum variance of the emission in the FOV, demonstrate the presence of the signal over both umbral and penumbral regions of analysed sunspots, providing us with the ROI for further analysis.

The global spatially integrated wavelet power spectra of the signals coming from the selected ROI (Figure 5) show the presence of five-minute oscillations. There are also 3- and 15-minute peaks in the spectra. (We do not need to estimate the probability of false

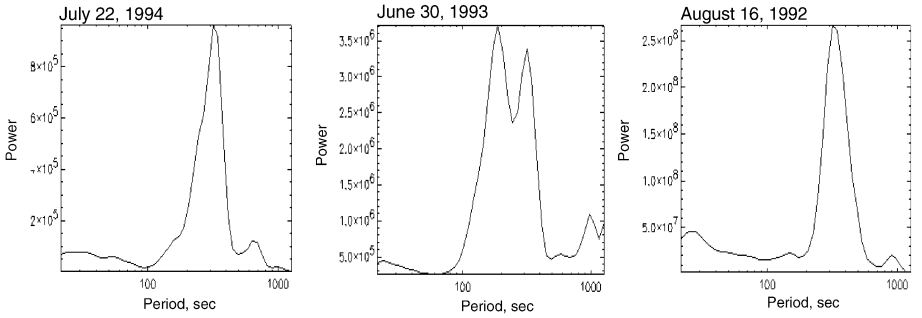

Figure 5 The spatially integrated global wavelet power spectra of the analysed temporal data cube (NoRH circular polarisation channel $V = R - L$) for 22 July 1994, 30 June 1993, and 16 August 1992.

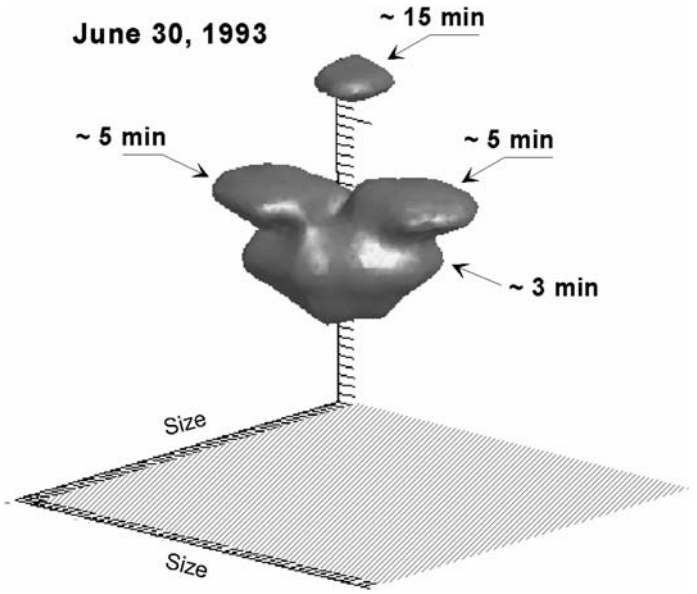

Figure 6 The broadband power cube of the data cube obtained on 30 June 1993 in the circular polarisation channel ($V = R - L$) with NoRH.

detection, as the presence of the signal in the data will be confirmed or disproved by the following analysis.)

The spatial distribution of the oscillation power in the data set of 30 June 1993 is shown by the broadband power cube (Figure 6). It is clearly seen that the 3- and 15-minute oscillations are located at the centre of the microwave source, which lies over the sunspot's umbra, whereas the five-minute oscillations are offset from the centre of the microwave source. However, the broadband power cube does not give us information about the temporal evolution of the oscillations. Applying the PWF method to the analysed datasets, we construct dynamical narrowband maps of the data cubes for the three significant periodicities found.

Narrowband power maps showing the spatial distribution of the 3-, 5-, and 15-minute oscillations in the analysed data cubes are given in Figure 7. According to the maps, there is an obvious difference in the position and shapes of the spatial sources of the detected periodicities. The size, shape, and positioning of all three sources coincide in the data of 22 July 1994 (Figure 7, upper panels) only. For the data set of 30 June 1993 (Figure 7, middle panels), the source of three-minute oscillations is situated at the central part of the integrated microwave image. The source of the 15-minute oscillations is situated at the centre of the integrated image too. However, the source of five-minute oscillations forms two patches of about 15″ in size. The five-minute oscillation sources seem to be situated at the umbra–penumbra boundary.

The phase narrowband maps of the event on 30 June 1993 reveal that the oscillations of each periodicity are in phase. This suggests that the observed oscillations are either standing or propagating along the line of sight. The analysis of the data of 16 August 1992 reveals similar morphology: The 3- and 15-minute oscillation sources are situated in the central part of the microwave source, but the five-minute oscillation source is found to be split into several patches situated at the umbra–penumbra boundary. The five-minute oscillations in some patches are antiphase with each other. This antiphase character of the five-minute os-

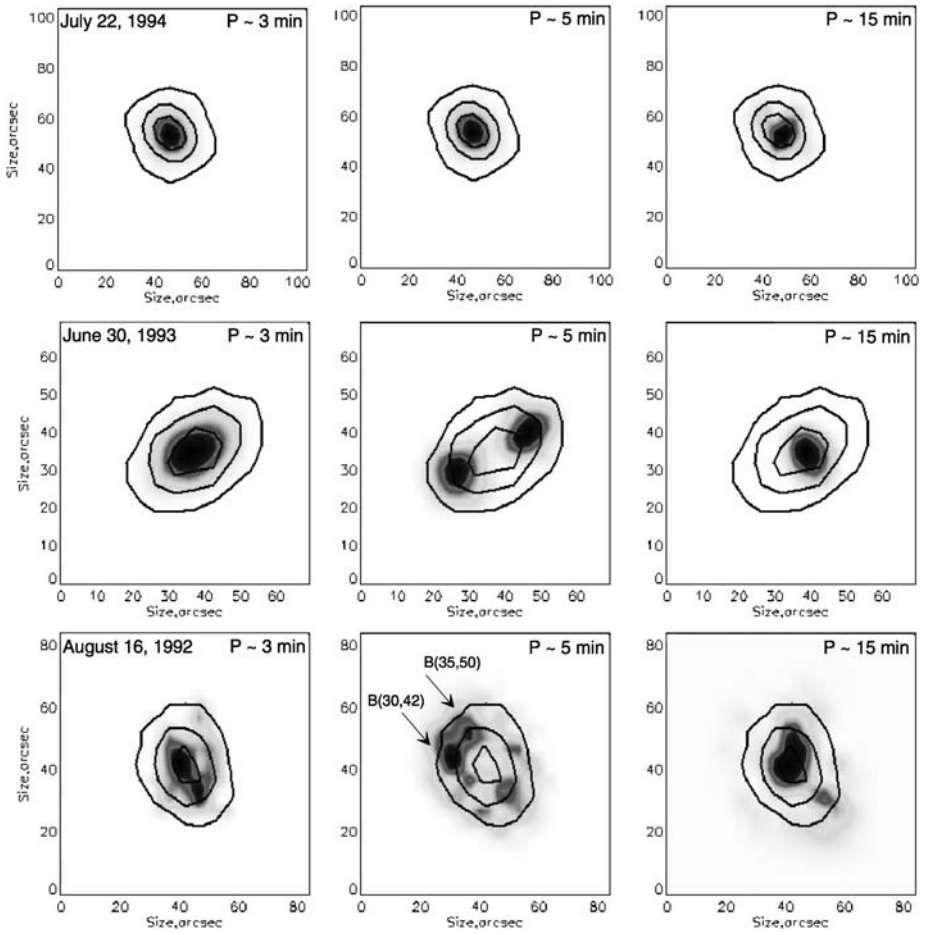

Figure 7 Narrowband power maps of the 3-, 5-, and 15-minute oscillation sources for the data of 22 July 1994, 30 June 1993, and 16 August 1992. The contours show the integrated microwave image. The arrows point out the patches of the antiphase five-minute oscillations.

cillations may reduce the observed power of the corresponding spectral peak in the spectrum of the signal integrated over the whole microwave source. This possibly explains the domination of the three-minute component in the spatially integrated signal.

5. Application to Coronal Loop Oscillations

In this section, we apply the PWF method to the analysis of the EUV data obtained with TRACE on 23 March 1999 for the active region 8496. The data were obtained in the 171 Å bandpass with a temporal cadence of about nine second and a 1″ pixel size. This data cube contains propagating longitudinal waves analysed by De Moortel, Hood, and Ireland (2002) with the use of the time–distance plots. Later on, Terradas, Oliver, and Ballester (2004) used these data to demonstrate the applicability of the EMD and CEOF methods. There were two

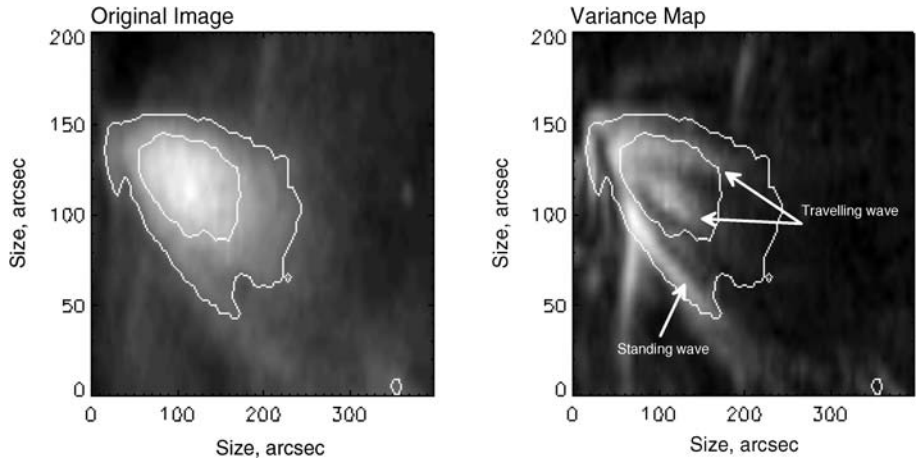

Figure 8 Left: The original image of the coronal loop. Right: Spatial variance of EUV emission with position of the loop details where observed standing (about 12 minutes) and travelling (about 5 minutes) waves are indicated.

distinct periodicities found in the data, about 3 and 11 minutes, in the form of both standing and propagating waves. Our aim is to confirm this finding with the PWF method.

The scheme of the application of the PWF method to this data cube is similar to that described earlier. First, the data are preprocessed with the use of the SSW IDL routines trace_prep, trace_align_cube, and align_cube_correl. A snapshot of the data cube is shown in the left panel of Figure 8. The broadband variance map is shown in the right panel of Figure 8. The strongest signal is seen to be localised along fine structures extended in the radial direction along the expected direction of the magnetic field. The prevailing periods of the oscillations present in the data were determined with the use of the global spatially integrated wavelet power spectrum and are found to be 5, 8, and 12 minutes. In addition, the analysed date cube was found to have strong high-frequency noise. For each of the 5- and 12-minute oscillations we constructed a sequence of the amplitude narrowband maps shown in Figure 9. It is evident that five-minute oscillations are amplitude variations propagating outwards along the same fine structures that are highlighted in Figure 8. The longer period oscillations, with a period of about 12 minutes, are seen to be situated near the outer edges of the loop as a nonpropagating wave, either standing or propagating along the line of sight. In those regions, the phase changes periodically without any movement of the nodes and extrema. A similar effect has already been found by Terradas, Oliver, and Ballester (2004) with the use of EMD and CEOF methods.

6. Conclusions

The main aim of this work was the development and testing of a method for the analysis of astronomical (in particular, solar) dynamical imaging data sets: the pixelised wavelet filtering method. The PWF method is a development of the wavelet technique proposed by De Moortel and McAteer (2004). The main novel element of this technique is the possibility of obtaining dynamical amplitude and phase narrowband maps (or movies), which provide us with information about the wave type (propagating or standing in the FOV) and allow us to study the temporal–spatial structure of quasi-harmonic signals. The dynamical narrowband

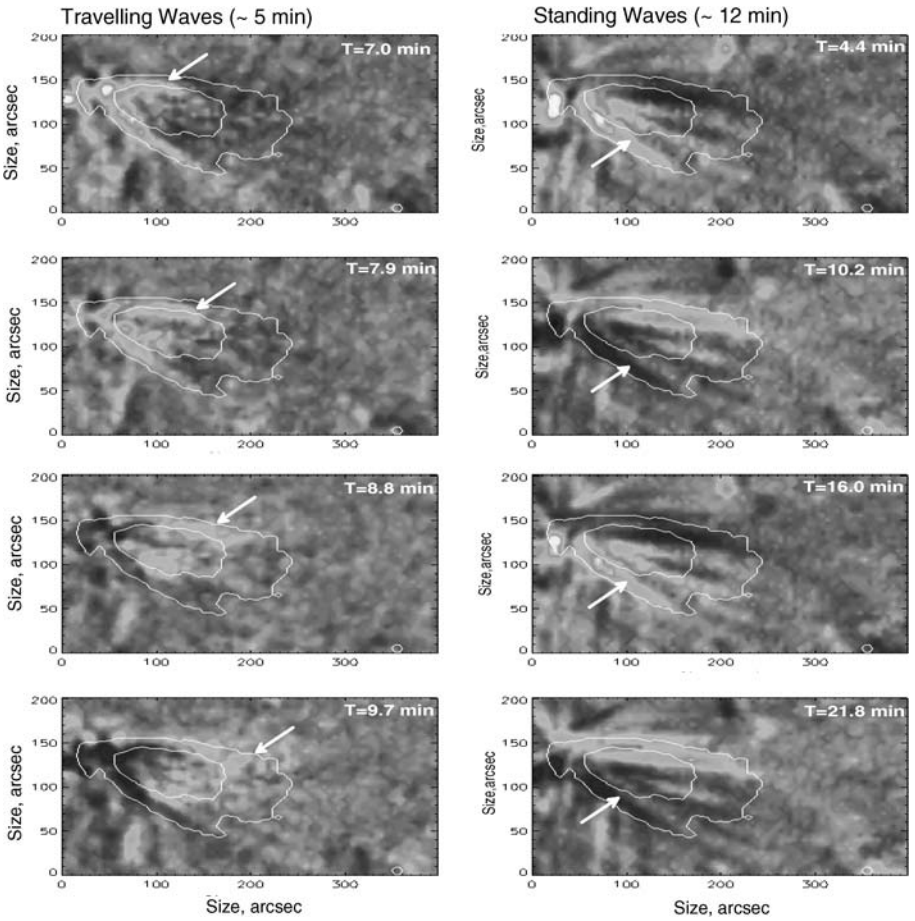

Figure 9 The snapshots of the amplitude distribution of the propagating (with periods of about five minutes) and nonpropagating (with periods of about 12 minutes) waves along an EUV coronal loop at different instants of time. The arrows point out the oscillation locations. The contours show the location of the loop.

maps can also be visualised by a sequence of narrowband maps calculated at certain instants of time.

Testing the PWF method with artificial test data sets that contained standing and propagating harmonic waves demonstrated its efficiency and robustness in the detection of the periodicities, identification of their type, and the determination of the spatial location of their sources.

The application of the PWF method to the analysis of sunspot oscillations gives us narrowband maps of temporal sequences of 2D images (data cubes) obtained in the microwave band with NoRH. The PWF analysis revealed that the 3-, 5-, and 15-minute periodicities, dominating the global spectrum of the oscillations, have a quite different spatial distribution over the sunspot. The 3- and 15-minute oscillations are situated in the umbra, whereas the sources of 5-minute oscillations are localised at small-size patches at the umbra – penumbra boundary. A similar spatial distribution of sunspot oscillations was observed by Zhugzhda, Balthasar, and Staude (2000) and Nindos *et al.* (2002).

Applying the PWF method to the coronal data sets obtained with TRACE in the EUV 171 Å band, we obtained the spatial structure of the previously found 5- and 12-minute oscillations of the EUV intensity. The five-minute waves, propagating along the FOV, are situated in narrow threads extended along the magnetic field. The 12-minute oscillations are observed to be nonpropagating in the FOV and also situated in the narrow magnetic field-aligned threads near the external boundaries of the magnetic fan coronal structure. Our results confirm the findings of Terradas, Oliver, and Ballester (2004) with the EMD and CEOF methods. As those methods are not well understood and have not become popular in the solar physics community, the confirmation of this finding with a well-understood and popular Morlet wavelet technique is of particular importance.

The possible interpretation of the observed phenomena will be discussed elsewhere.

In comparison with the alternative techniques already applied in coronal seismology and other solar atmospheric wave studies, such as the EMD and CEOF methods (Terradas, Oliver, and Ballester, 2004), the PWF method has the following advantages: We know the exact boundaries of the frequency bands of the narrowband signal (as a multiple of two, and as any other, including an arbitrarily chosen one); we can prescribe a certain frequency (or a band) to be extracted and analysed. Also, by varying the wavenumber in the mother wavelet function (and, possibly, changing the mother wavelet function itself) the PWF method allows us to vary the frequency–temporal resolution of the wavelets as a frequency filter. Such flexibility is absent from the aforementioned alternative methods, where the internal frequencies of the obtained elementary functions should be determined with other spectral methods, *e.g.* with the Fourier transform.

Thus, we believe that the PWF method discussed here has a number of important advantages for the analysis of imaging data. Possible applications of the PWF method include the study of the interaction of various wave modes, revealing the time-dependent energy exchange between the modes. The PWF method can easily be modified to show the spatial distribution of phase speeds (projected on the FOV plane) of detected wave processes. The PWF method can work in combination with the pre-analysis period-mapping technique developed by Nakariakov and King (2007) for the automated detection of wave and oscillatory processes in coronal EUV imaging data cubes.

Acknowledgements The authors thank Dr. Uralov for useful discussions. R.A.S. is grateful to the Russian Fund of Fundamental Research for the funding provided under Grant Nos. N04-02-39003 and N05-07-90147. The authors thank the Royal Society for the support through the International Incoming Short Visit scheme. Wavelet software was provided by C. Torrence and G. Compo (http://paos.colorado.edu/research/wavelets).

References

Baudin, F., Bocchialini, K., Koutchmy, S.: 1996, *Astron. Astrophys.* **314**, L9.
Christopoulou, E.B., Skodras, A., Georgakilas, A.A., Koutchmy, S.: 2003, *Astrophys. J.* **591**, 416.
De Moortel, I., Hood, A.W., Ireland, J.: 2002, *Astron. Astrophys.* **381**, 311.
De Moortel, I., Ireland, J., Walsh, R.W.: 2000, *Astron. Astrophys.* **355**, L23.
De Moortel, I., McAteer, R.T.J.: 2004, *Solar Phys.* **223**, 1.
Gelfreikh, G.B., Grechnev, V., Kosugi, T., Shibasaki, K.: 1999, *Solar Phys.* **185**, 177.
Golyandina, N., Nekrutkin, V., Zhiglyavsky, A.: 2001, *Analysis of Time Series Structure. SSA and Related Techniques*, Chapman and Hall/CRC, London/Boca Raton.
Grechnev, V.V.: 2003, *Solar Phys.* **213**, 103.
Huang, N.E., Shen, Z., Long, S.R.: 1999, *Annu. Rev. Fluid Mech.* **31**, 417.
Ireland, J., Walsh, R.W., Harrison, R.A., Priest, E.R.: 1999, *Astron. Astrophys.* **347**, 355.
King, D.B., Nakariakov, V.M., Deluca, E.E., Golub, L., McClements, K.G.: 2003, *Astron. Astrophys.* **404**, L1.

Marsh, M.S., Walsh, R.W., De Moortel, I., Ireland, J.: 2003, *Astron. Astrophys.* **404**, L37.
Meyer, Y., Roques, S. (eds.): 1993, *Proceedings of the International Conference: Wavelets and Applications*, Editions Frontieres, Gif-sur-Yvette.
Milovanov, A.V., Zelenyj, L.M.: 1993, *Phys. Fluids B* **5**, 2609.
Nakariakov, V.M., King, D.B.: 2007, *Solar Phys.* **241**, 397.
Nakariakov, V.M., Verwichte, E.: 2005, *Living Rev. Solar Phys.* **2**, 3. http://www.livingreviews.org/lrsp-2005-3.
Nindos, A., Alissandrakis, C.E., Gelfreikh, G.B., Bogod, V.M., Gontikakis, C.: 2002, *Astron. Astrophys.* **386**, 658.
Terradas, J., Oliver, R., Ballester, J.L.: 2004, *Astrophys. J.* **614**, 435.
Torrence, C., Compo, G.P.: 1998, *Bull. Am. Meteorol. Soc.* **79**, 61.
Weng, H., Lau, K.-M.: 1994, *J. Atmos. Sci.* **51**, 2523.
Zhugzhda, Y.D., Balthasar, H., Staude, J.: 2000, *Astron. Astrophys.* **355**, 347.